



Supplement of

A research product for tropospheric NO₂ columns from Geostationary Environment Monitoring Spectrometer based on Peking University OMI NO₂ algorithm

Yuhang Zhang et al.

Correspondence to: Jintai Lin (linjt@pku.edu.cn)

The copyright of individual parts of the supplement might differ from the article licence.

1 **1. Derivation of the assumption in the total NO₂ SCD correction method**

2 In principle, the corrected total NO₂ SCDs by combining GEMS and TROPOMI observations
3 should be:

$$\begin{aligned}
 4 \quad \text{SCD}_{\text{total},h}^{\text{corrected}} &= \text{SCD}_{\text{total},h}^{\text{GEMS}} + \left(\frac{\text{SCD}_{\text{total},h}^{\text{TROPOMI}}}{\text{AMF}_{\text{total},h}^{\text{TROPOMI}}} - \frac{\text{SCD}_{\text{total},h}^{\text{GEMS}}}{\text{AMF}_{\text{total},h}^{\text{GEMS}}} \right) \cdot \text{AMF}_{\text{total},h}^{\text{GEMS}} \\
 5 \quad &= \text{SCD}_{\text{total},h}^{\text{TROPOMI}} \cdot \frac{\text{AMF}_{\text{total},h}^{\text{GEMS}}}{\text{AMF}_{\text{total},h}^{\text{TROPOMI}}} \\
 6 \quad &= \text{SCD}_{\text{total},h}^{\text{TROPOMI}} \cdot \frac{\text{AMFgeo}_h^{\text{GEMS}} \int_0^\infty w_h^{\text{GEMS}}(z)S(z)dz}{\text{AMFgeo}_h^{\text{TROPOMI}} \int_0^\infty w_h^{\text{TROPOMI}}(z)S(z)dz} \\
 7 \quad &= \text{SCD}_{\text{total},h}^{\text{TROPOMI}} \cdot \frac{\text{AMFgeo}_h^{\text{GEMS}} \left(\int_{z_T}^\infty w_h^{\text{GEMS}}(z)S(z)dz + \int_0^{z_T} w_h^{\text{GEMS}}(z)S(z)dz \right)}{\text{AMFgeo}_h^{\text{TROPOMI}} \left(\int_{z_T}^\infty w_h^{\text{TROPOMI}}(z)S(z)dz + \int_0^{z_T} w_h^{\text{TROPOMI}}(z)S(z)dz \right)} \\
 8 \quad &\approx \text{SCD}_{\text{total},h}^{\text{TROPOMI}} \cdot \frac{\text{AMFgeo}_h^{\text{GEMS}} \left(1 + \int_0^{z_T} w_h^{\text{GEMS}}(z)S(z)dz \right)}{\text{AMFgeo}_h^{\text{TROPOMI}} \left(1 + \int_0^{z_T} w_h^{\text{TROPOMI}}(z)S(z)dz \right)} \\
 9 \quad &= \text{SCD}_{\text{total},h}^{\text{TROPOMI}} \cdot \frac{\text{AMFgeo}_h^{\text{GEMS}}}{\text{AMFgeo}_h^{\text{TROPOMI}}} \cdot \frac{1 + \frac{\text{AMF}_h^{\text{GEMS}}}{\text{AMFgeo}_h^{\text{GEMS}}}}{1 + \frac{\text{AMF}_h^{\text{TROPOMI}}}{\text{AMFgeo}_h^{\text{TROPOMI}}}}
 \end{aligned}$$

10 In our actual correction, we define and assume the “approximation ratio” as:

$$11 \quad \frac{1 + \frac{\text{AMF}_h^{\text{GEMS}}}{\text{AMFgeo}_h^{\text{GEMS}}}}{1 + \frac{\text{AMF}_h^{\text{TROPOMI}}}{\text{AMFgeo}_h^{\text{TROPOMI}}}} \approx 1$$

12 So that the corrected NO₂ SCDs become:

$$13 \quad \text{SCD}_{\text{total},h}^{\text{corrected}} = \text{SCD}_{\text{total},h}^{\text{TROPOMI}} \cdot \frac{\text{AMFgeo}_h^{\text{GEMS}}}{\text{AMFgeo}_h^{\text{TROPOMI}}}$$

14 Figure S2 shows the spatial distribution of mean “approximation ratio” in June 2021 which we
15 assume to be 1. The “approximation ratio” is in the range of 0.9 – 1.1 in most central and eastern parts
16 of GEMS FOV, but is smaller in the western and northwestern parts (around 0.8 in most places, with a
17 minimum value around 0.7).

18 **2. MAX-DOAS instruments**

19 There are four instruments installed in various areas of Shanghai. The instrument located in the
20 campus of Fudan University is in the urban center of Shanghai (31.34°N, 121.52°E). The telescope’s

21 azimuth angle is 0° , and the scattered sunlight is measured at ten elevation angles of 2° , 3° , 5° , 7° , 10° ,
22 15° , 20° , 30° , 45° and 90° within 15 minutes. The Nanhui site is in the suburban area (31.06°N , 121.80°E)
23 and about 10 km southeast to the center of Shanghai. The azimuth angle is set to 2° and it takes about 15
24 minutes for a full cycle with elevation angles of 2° , 3° , 5° , 7° , 9° , 12° , 15° , 20° , 30° , 45° and 90° . The
25 Dianshan Lake site is located near the Dianshan Lake Scenic Area (31.10°N , 120.98°E), which is at the
26 junction of Suzhou and Shanghai. The Chongming site is on the Chongming Island (31.50°N , 121.82°E)
27 of Shanghai, which is China's third largest island and located in Yangtze River estuary. The instruments
28 at Dianshan Lake (suburban) and Chongming (rural) sites are operated in the same way as that in the
29 Nanhui site, except with a fixed azimuth angle at 5° (Zhang et al., 2021; Zhang et al., 2022a; Zhang et
30 al., 2022b; Zhu et al., 2022).

31 The instrument operated in Xianghe is designed by BIRA-IASB and run by both BIRA-IASB and
32 CAS-IAP. It is located in the suburban area (39.75°N , 116.96°E) of Xianghe county to the southwest of
33 Beijing. The telescope's azimuth direction is fixed to the north, and a full scan requiring about 15 minutes
34 comprises nine elevation angles: 2° , 4° , 6° , 8° , 10° , 12° , 15° , 30° and 90° (Clémer et al., 2010; Hendrick
35 et al., 2014).

36 The instrument in Xuzhou is set on the roof of the School of Environmental Science and Spatial
37 Informatics, China University of Mining and Technology (34.22°N , 117.14°E). It is located 6.5 km away
38 from the urban center of Xuzhou, and about 1 km south to the Yunlong Lake Scenic Area, which is a 5A
39 natural scenic area. It measures scattered sunlight every 5 minutes for five zenith angles: 5° , 10° , 20° ,
40 30° and 90° . This instrument is normally operated from 9:00 to 17:00 local solar time (LST) each day
41 (Liu et al., 2020).

42 The instrument in Hefei site was deployed in March 2008 and is run by Anhui Institute of Optics
43 and Fine Mechanics (AIOFM), Chinese Academy of Science (CAS). It is located outdoors in the campus
44 of AIOFM and about 10 km northwest to the center of Hefei city (31.91°N , 117.16°E). It takes 30 minutes
45 for a cycle to measure introduced scattered sunlight with sequential elevation angles of 3° , 5° , 10° , 20° ,
46 30° and 90° (Kanaya et al., 2014).

47 The Fukue and Cape Hedo sites are both remote sites located far away from the major cities
48 (32.75°N , 128.68°E and 26.87°N , 128.25°E , respectively). They are suitable for monitoring tropospheric
49 NO_2 in the background regions and outflow from Korea and China. Similar to the instrument at Hefei,

50 the scattered sunlight is measured by rotating a prism at six elevation angles 3°, 5°, 10°, 20°, 30° and 90°,
51 with 5 minutes for each angle and 30 minutes for a total (Kanaya et al., 2014; Choi et al., 2021).

52 **3. Discussion of the differences between POMINO-GEMS and POMINO-TROPOMI v1.2.2** 53 **tropospheric NO₂ VCDs**

54 The differences between POMINO-GEMS and POMINO-TROPOMI v1.2.2 tropospheric NO₂
55 VCDs are related to tropospheric NO₂ AMFs and SCDs. As shown in Figure S10, POMINO-GEMS
56 tropospheric NO₂ AMF is larger than POMINO-TROPOMI v1.2.2 in the western part of GEMS FOV,
57 except over major cities such as Urumqi in China and New Delhi in India, but is smaller in most of the
58 eastern part. Such AMF differences can be further separated into differences in geometric AMF and
59 scattering correction factor.

60 For a certain pixel and time, GEMS and TROPOMI have the same SZA but different VZAs and
61 thus different geometric AMFs. The GEMS geometric AMFs exhibit a circle-like spatial pattern,
62 increasing from less than 3 in the southeast to more than 5 in the northwest of GEMS FOV, corresponding
63 to the increase of VZA. In contrast, the TROPOMI geometric AMFs exhibit a different spatial pattern
64 with values varying from 2 to 3 (Figure S11). As a result, the GEMS geometric AMFs are larger than
65 those of TROPOMI in the northwest and smaller in the southeast of GEMS FOV.

66 The scattering correction factors of POMINO-GEMS and POMINO-TROPOMI v1.2.2 are different
67 as well. POMINO-GEMS explicitly employs CALIOP-corrected aerosol vertical profiles and re-
68 calculates cloud fraction and cloud pressure based on continuum reflectances and O₂-O₂ SCDs from
69 GEMS observations. By comparison, POMINO-TROPOMI v1.2.2 does not use CALIOP observations
70 to constrain aerosol vertical profiles; and it takes the FRESCO-wide cloud pressure data from the official
71 TROPOMI PAL v2.3.1 NO₂ product and re-calculates cloud fraction at 440 nm. Constraint by CALIOP
72 observations results in higher aerosol-concentrated layer heights (Liu et al., 2019), which enhances the
73 “screening” effect on the absorption by NO₂ and leads to lower scattering correction factors over polluted
74 regions such as eastern China (Figure S12). Higher scattering correction factors of POMINO-GEMS
75 occur over remote areas such as the Pacific Ocean.

76 In addition to tropospheric NO₂ AMFs, the differences in tropospheric NO₂ SCDs between
77 POMINO-GEMS and POMINO-TROPOMI v1.2.2 also contribute to their differences in VCDs. In the
78 correction for total NO₂ SCDs, the corrected total GCDs of GEMS are forced to agree with TROPOMI

79 PAL v2.3.1 GCDs at the overpass time of TROPOMI. Thus, the difference in geometry between GEMS
80 and TROPOMI leads to different total NO₂ SCDs and hence tropospheric SCDs. In Figure S13c and d,
81 the spatial distribution of differences in tropospheric NO₂ SCDs between POMINO-GEMS and
82 POMINO-TROPOMI v1.2.2 shows positive values over northwestern part and negative values over
83 southeastern part of GEMS FOV.

84 **4. Supplemental tables and figures**

85 **Table S1. Basic information of TROPOMI, OMI, GOME-2 and GEMS instruments**

Instrument	Spacecraft	Equator crossing time	Spectral range	Nominal spatial resolution
TROPOMI	Sentinel-5 Precursor (ESA)	13:30 LT	270-500 nm;	$3.5 \times 7 \text{ km}^2$ $(3.5 \times 5.5 \text{ km}^2 \text{ since } 6^{\text{th}} \text{ Aug. } 2019)$
			675-775 nm;	
			2305-2385 nm	
OMI	EOS-Aura (NASA)	13:45 LT	270-500 nm	$13 \times 24 \text{ km}^2$
GOME-2	MetOp-A (EUMETSAT)	9:30 LT	240-790 nm	$80 \times 40 \text{ km}^2$
GEMS	Geostationary Korea Multi-Purpose Satellite- 2B (GK-2B)	128.2°E over the equator	300-500 nm	$7 \times 8 \text{ km}^2$ (gases);
				$3.5 \times 8 \text{ km}^2$ (aerosols)

86

87

88 **Table S2. Specifics for the NO₂ SCD retrieval of TROPOMI PAL v2.3.1 and GEMS v1.0**

89 **operational products**

	TROPOMI PAL v2.3.1	GEMS v1.0
Type of DOAS fit	Intensity fit	Optical fit
χ^2 minimization method	Levenberg-Marquardt	Levenberg-Marquardt
Wavelength range	405-465 nm	432-450 nm
Solar reference spectrum	E_{ref} from Chance and Kurucz (2010)	E_{ref} from Chance and Kurucz (2010)
NO ₂ reference spectrum	σ_{NO_2} at 220 K from Vandaele et al. (1998)	σ_{NO_2} at 220 K from Vandaele et al. (1998)
O ₃ reference spectrum	σ_{O_3} at 243 K from Serdyuchenko et al. (2014)	σ_{O_3} from 243 and 293 K from Bogumil et al. (2003)
O ₂ -O ₂ reference spectrum	$\sigma_{\text{O}_2-\text{O}_2}$ at 293 K from Thalman and Volkamer (2013)	$\sigma_{\text{O}_2-\text{O}_2}$ at 293 K from Thalman and Volkamer (2013)
Water vapor reference spectrum	$\sigma_{\text{H}_2\text{O}_{\text{vap}}}$ at 293 K from	Not yet applied

	HITRAN 2012 data	
Liquid water reference spectrum	$\sigma_{\text{H}_2\text{O}_{\text{liq}}}$ from Pope and Fry (1997)	Not yet applied
Ring reference spectrum	I_{ring} derived following Chance and Spurr (1997)	σ_{ring} derived following Chance and Spurr (1997)

90

91

92

Table S3. Ground based MAX-DOAS measurements

Site name	Type	Geolocation	Measurement time
Fudan University	Urban	121.52°E, 31.34°N	1 June – 31 August 2021
Xuzhou	Suburban	117.14°E, 34.22°N	1 June – 31 August 2021
Hefei	Suburban	117.16°E, 31.91°N	1 June – 30 June 2021
Nanhui	Suburban	121.80°E, 31.06°N	1 June – 31 August 2021
Xianghe	Suburban	116.96°E, 39.75°N	1 June – 31 August 2021
Dianshan Lake	Suburban	120.98°E, 31.30°N	1 June – 31 August 2021
Chongming	Rural	121.82°E, 31.50°N	1 June – 31 August 2021
Fukue	Remote	128.68°E, 32.75°N	1 June – 31 August 2021
Cape Hedo	Remote	128.25°E, 26.87°N	1 June – 31 August 2021

93

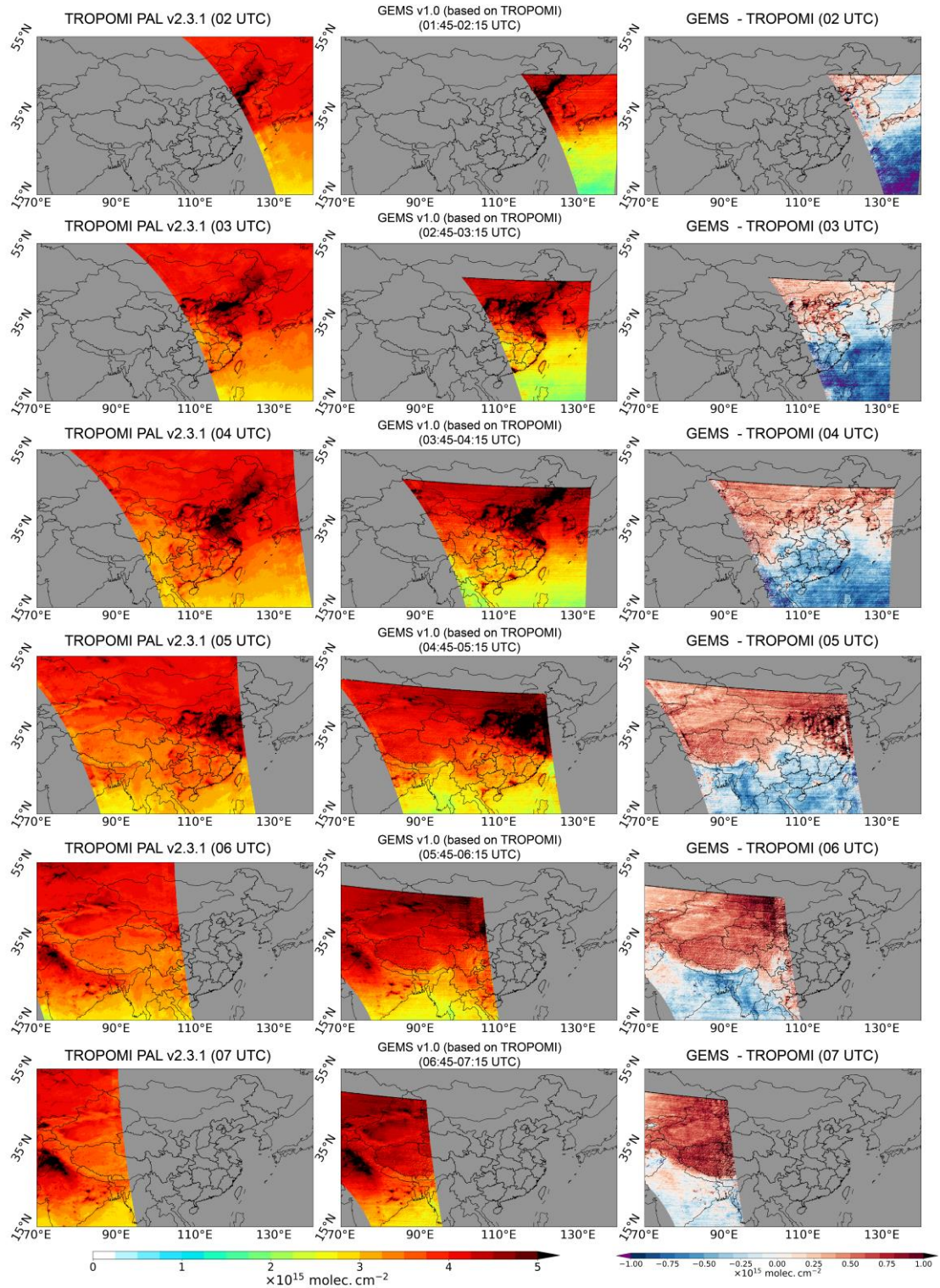
94

95

Table S4. Evaluation of surface NO₂ concentrations derived from POMINO-GEMS with total

SCD correction and POMINO-GEMS without correction using MEE measurements

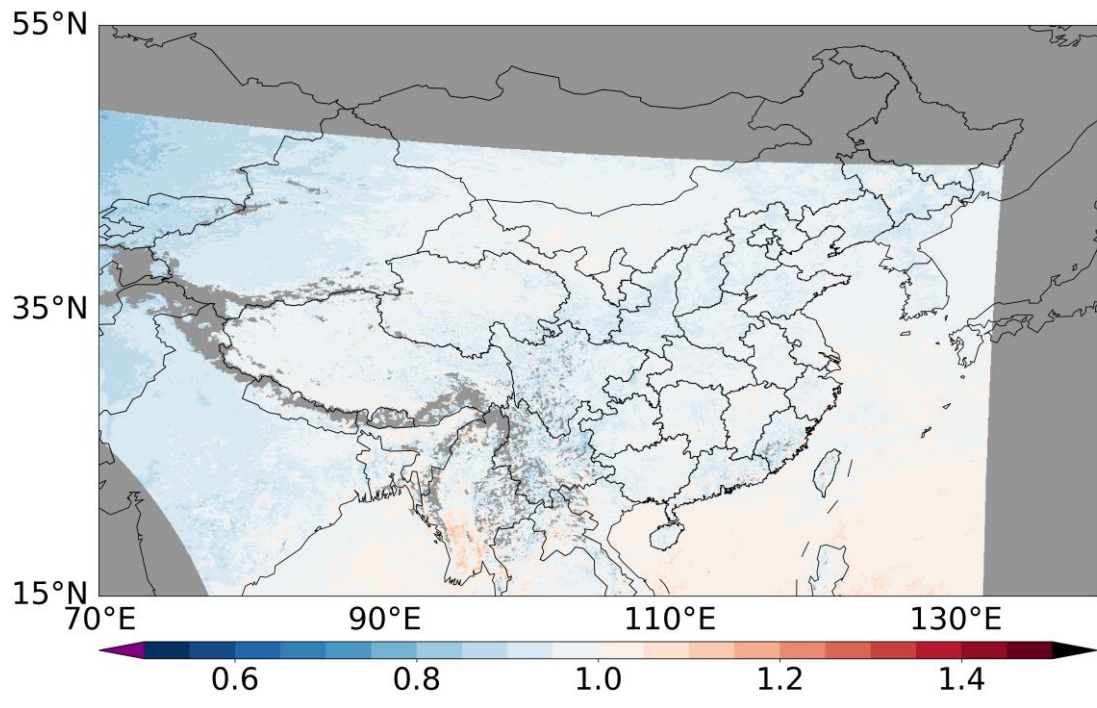
MEE sites	POMINO-GEMS		POMINO-GEMS	
	with total SCD correction		without total SCD correction	
	<i>R</i>	NMB	<i>R</i>	NMB
All	0.97	-34.4%	0.97	-27.1%
Urban	0.97	-28.7%	0.97	-19.8%
Suburban	0.97	-42.8%	0.97	-38.0%
Rural	0.96	-48.4%	0.96	-44.4%



98

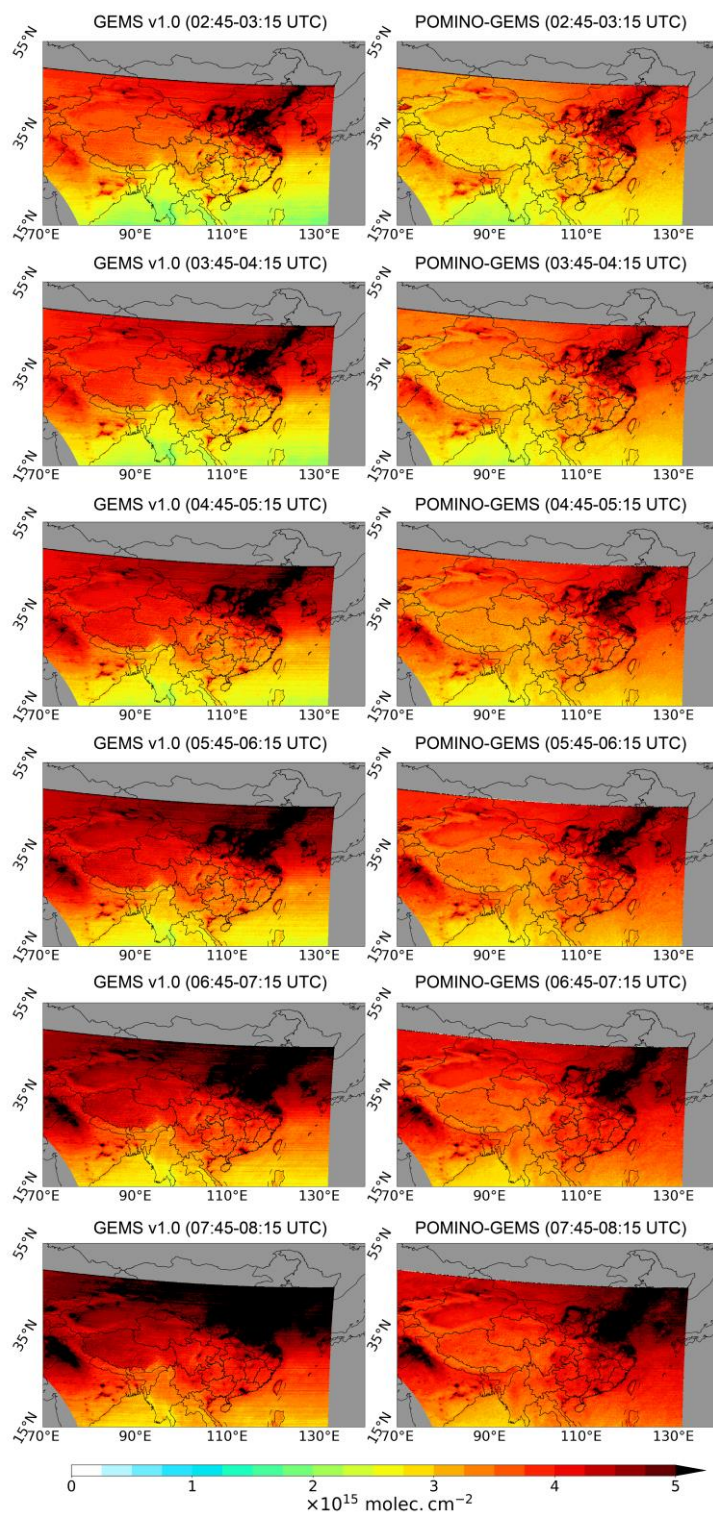
99 **Figure S1. Spatial distribution of monthly mean total NO₂ GCDs at each hour on a 0.05° × 0.05° grid in June**
 100 **2021. Left column, TROPOMI PAL v2.3.1 product; middle column, GEMS v1.0 product that**
 101 **spatiotemporally matches with TROPOMI; right column, the absolute differences of GEMS total NO₂**
 102 **GCDs from those of TROPOMI. The regions in grey mean there are no valid observations.**

103



104
105
106
107

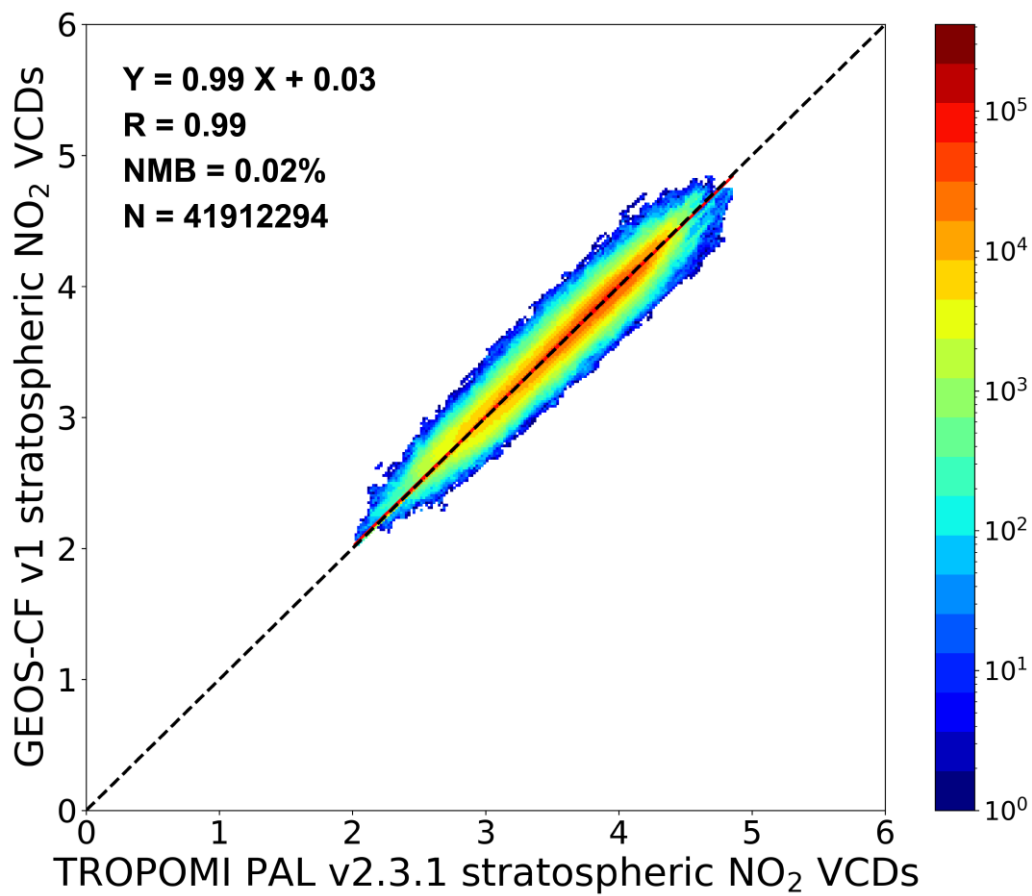
Figure S2. Spatial distribution of mean approximation ratios on a $0.05^\circ \times 0.05^\circ$ grid in June 2021. The regions in grey mean there are no valid NO_2 observations.



108

109 **Figure S3. Spatial distribution of monthly mean total NO₂ GCDs at each hour on a 0.05° × 0.05° grid in June**
 110 **2021. Left column, official GEMS v1.0 product; right column, corrected POMINO-GEMS product. The**
 111 **regions in grey mean there are no valid observations.**

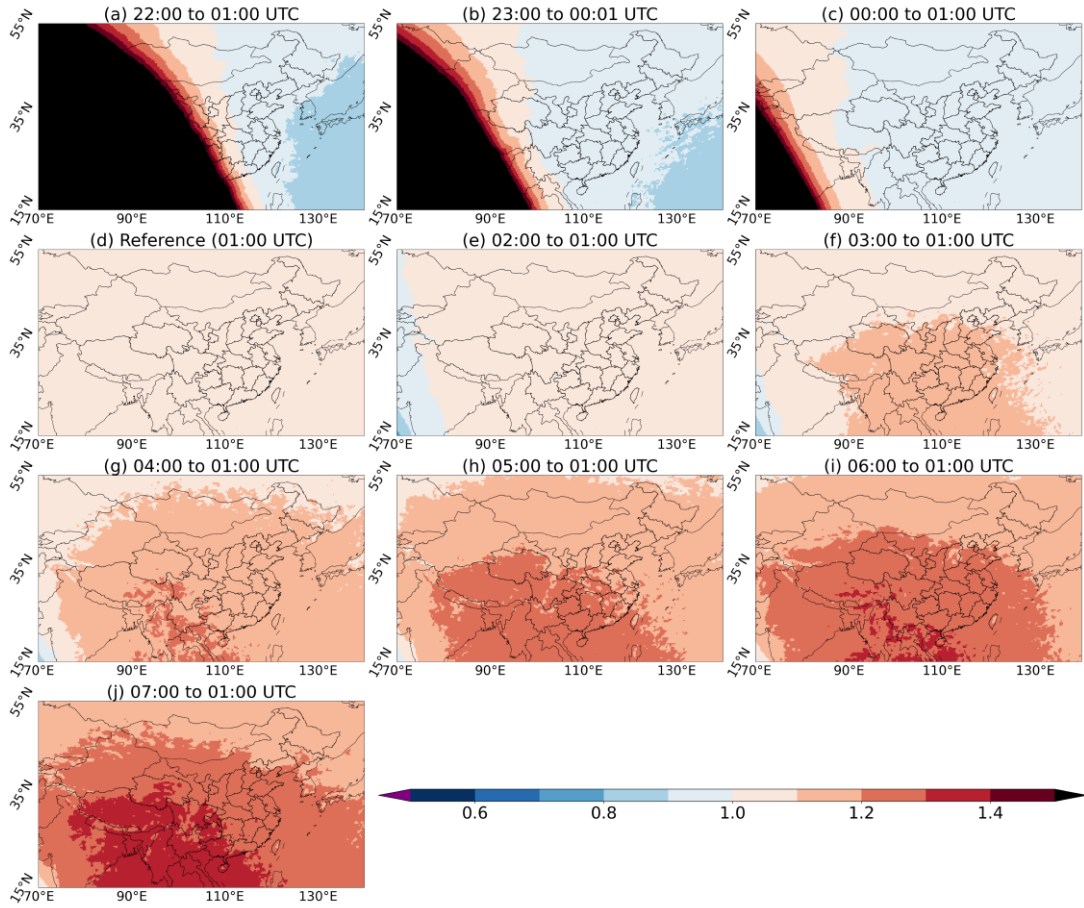
112



113

114 **Figure S4. Scatterplot for stratospheric NO₂ VCDs between GEOS-CF v1 and TROPOMI PAL v2.3.1**
 115 **products in June 2021. Colors represent the data density.**

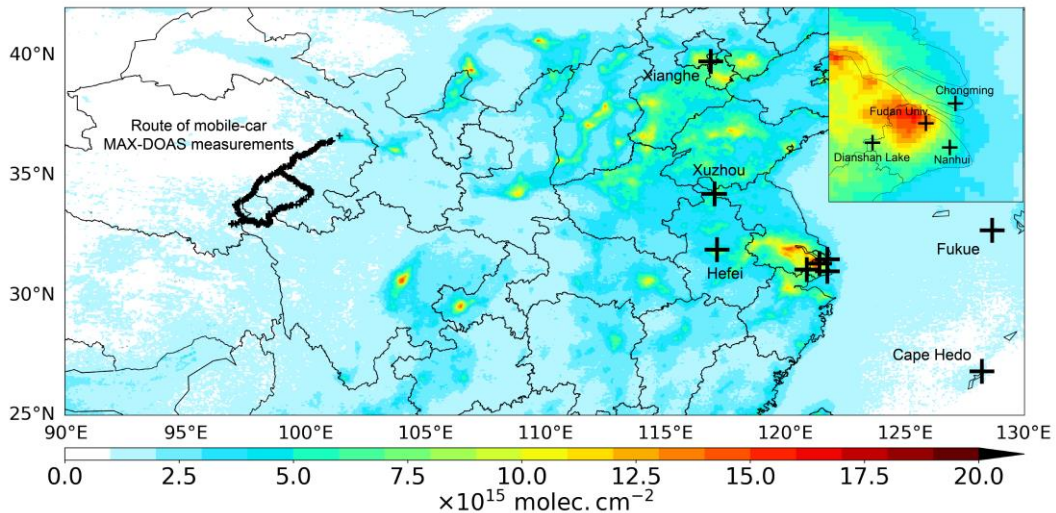
116



117

118 **Figure S5. Spatial distribution of GEOS-CF derived stratospheric NO₂ ratio at each hour to the reference**
 119 **hour (01:00 UTC) on a 0.05° × 0.05° grid in June 2021.**

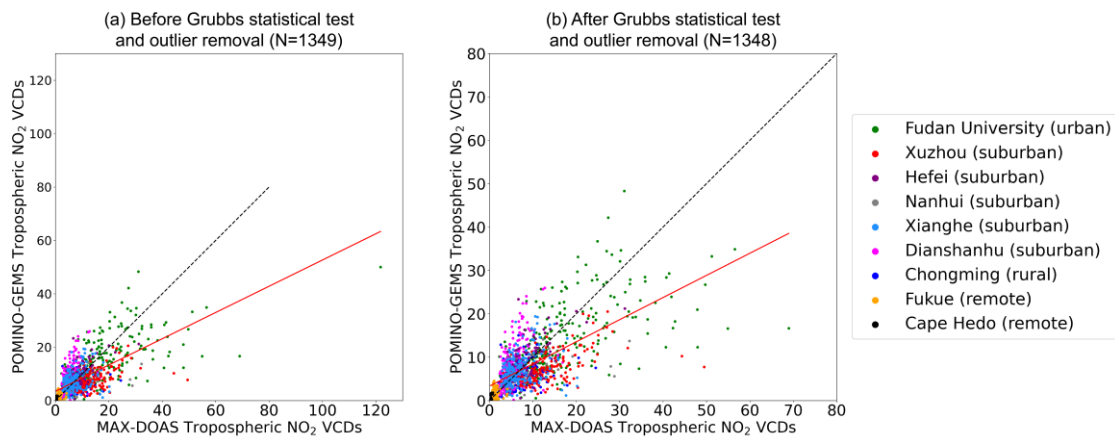
120



121

122 **Figure S6. Spatial distribution of ground-based MAX-DOAS sites and the route of mobile-car MAX-DOAS**
 123 **measurements used in this study. Overlaid in the background is the spatial distribution of POMINO-GEMS**
 124 **tropospheric NO₂ VCDs in JJA 2021 on a 0.05° × 0.05° grid.**

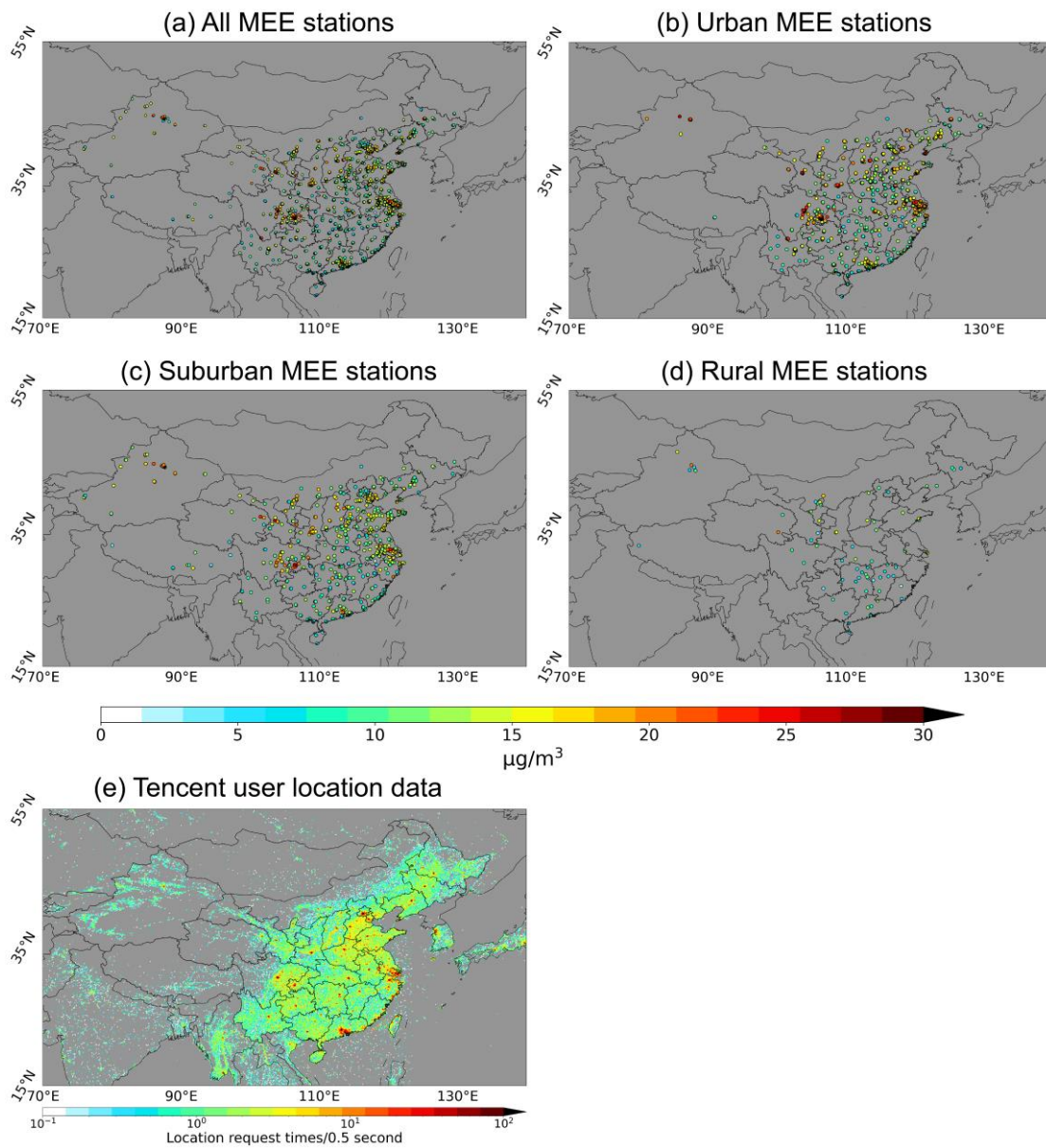
125



126

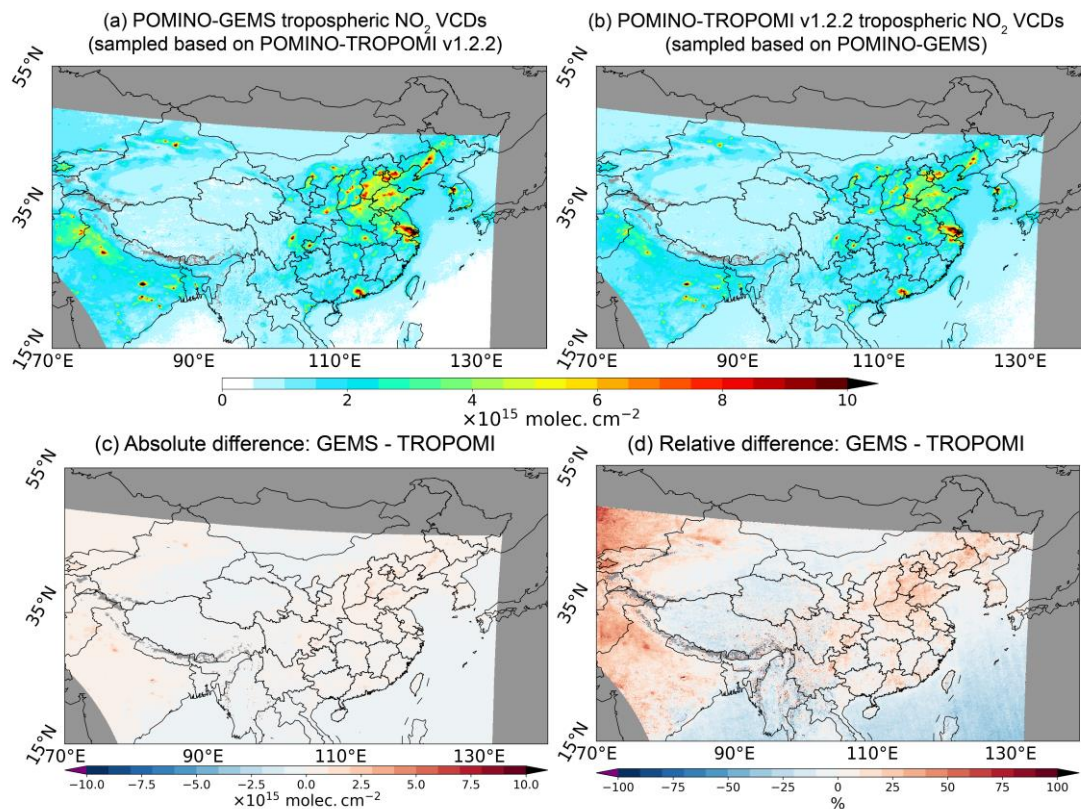
127 **Figure S7. Scatterplots for tropospheric NO₂ VCDs ($\times 10^{15}$ molec. cm⁻²) between MAX-DOAS and**
128 **POMINO-GEMS at all GEMS observation hours in JJA 2021 (a) before and (b) after performing Grubbs**
129 **statistical test and outlier removal. Only one outlier is identified.**

130



131
 132 **Figure S8. Spatial distribution of mean MEE surface NO₂ concentrations in JJA 2021 at (a) all, (b) urban,**
 133 **(c) suburban and (d) rural sites. The classification is based on (e) mean Tencent user location data from 31**
 134 **August to 30 September 2021 in China. The regions in grey mean there are no valid observations.**

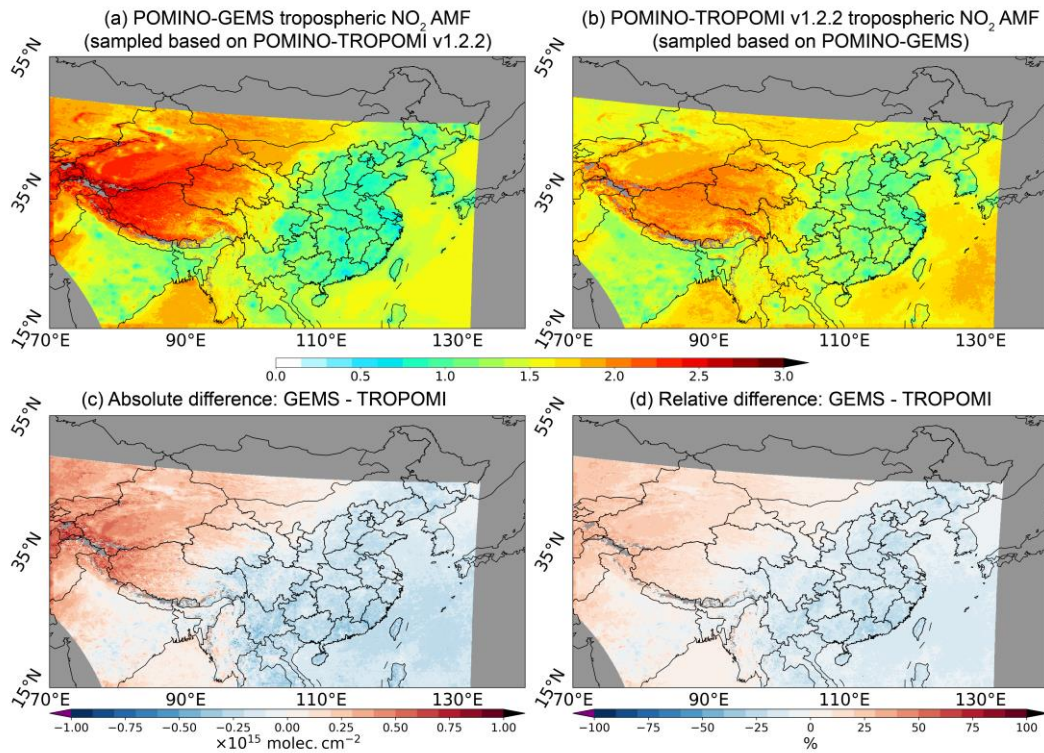
135



136

137 **Figure S9. Spatial distribution of (a) POMINO-GEMS and (b) POMINO-TROPOMI v1.2.2 tropospheric**
 138 **NO₂ VCDs on a 0.05° × 0.05° grid in JJA 2021. (c) and (d) are absolute and relative differences of POMINO-**
 139 **GEMS tropospheric NO₂ VCDs from those of POMINO-TROPOMI v1.2.2, respectively. Data are sampled**
 140 **from locations and times with valid data in both POMINO-GEMS and POMINO-TROPOMI v1.2.2. The**
 141 **regions in grey mean there are no valid observations.**

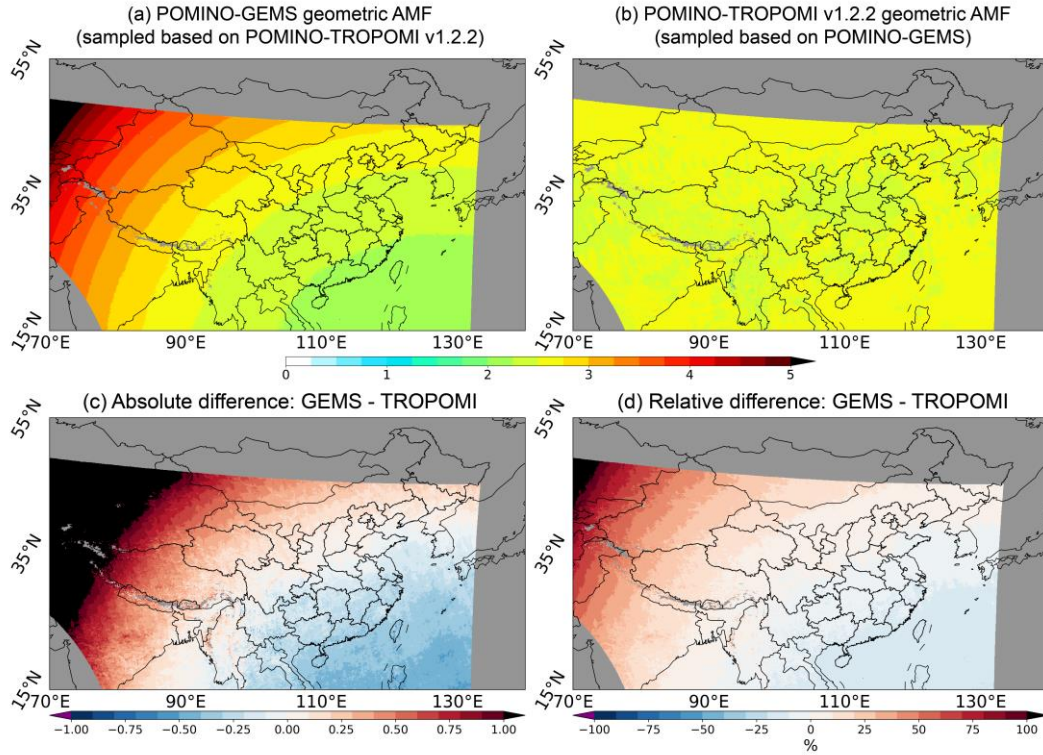
142



143

144 **Figure S10. Spatial distribution of (a) POMINO-GEMS and (b) POMINO-TROPOMI v1.2.2 tropospheric**
 145 **NO₂ AMFs on a $0.05^\circ \times 0.05^\circ$ grid in JJA 2021. (c) and (d) are absolute and relative differences of POMINO-**
 146 **GEMS tropospheric NO₂ AMFs from those of POMINO-TROPOMI v1.2.2, respectively. Data are sampled**
 147 **from locations and times with valid NO₂ VCD data in both POMINO-GEMS and POMINO-TROPOMI**
 148 **v1.2.2. The regions in grey mean there are no valid NO₂ observations.**

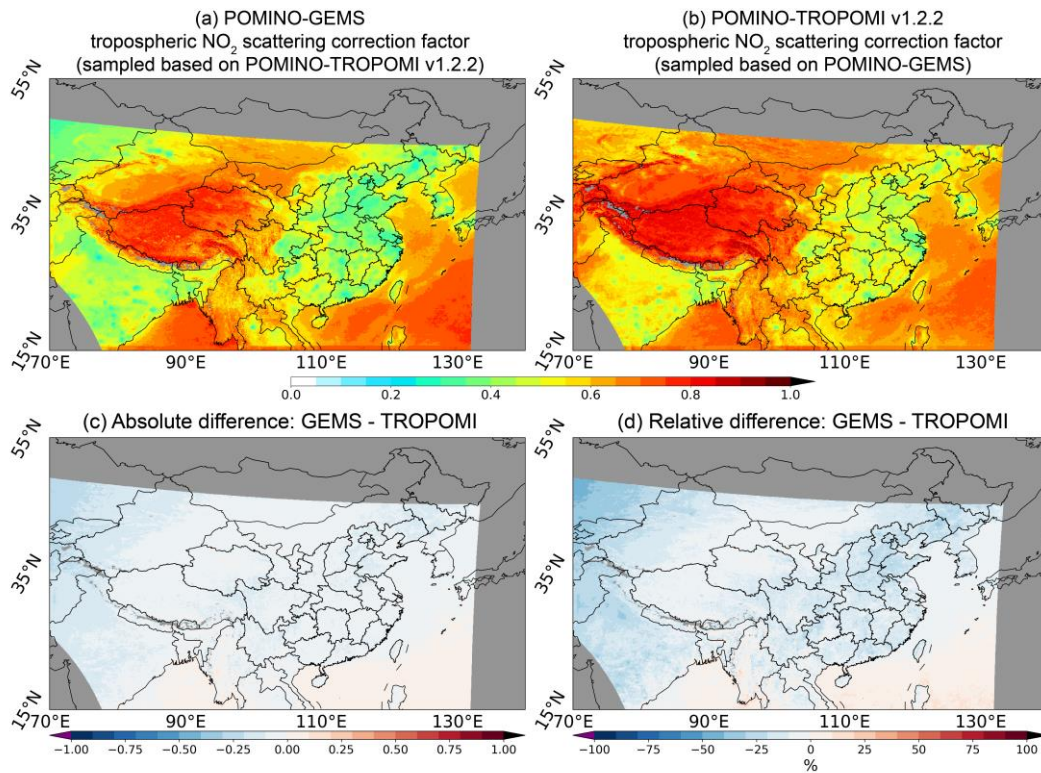
149



150

151 **Figure S11. Spatial distribution of (a) POMINO-GEMS and (b) POMINO-TROPOMI v1.2.2 geometric**
 152 **AMFs on a $0.05^\circ \times 0.05^\circ$ grid in JJA 2021. (c) and (d) are absolute and relative differences of POMINO-**
 153 **GEMS geometric AMFs from those of POMINO-TROPOMI v1.2.2, respectively. Data are sampled from**
 154 **locations and times with valid NO₂ VCD data in both POMINO-GEMS and POMINO-TROPOMI v1.2.2.**
 155 **The regions in grey mean there are no valid NO₂ observations.**

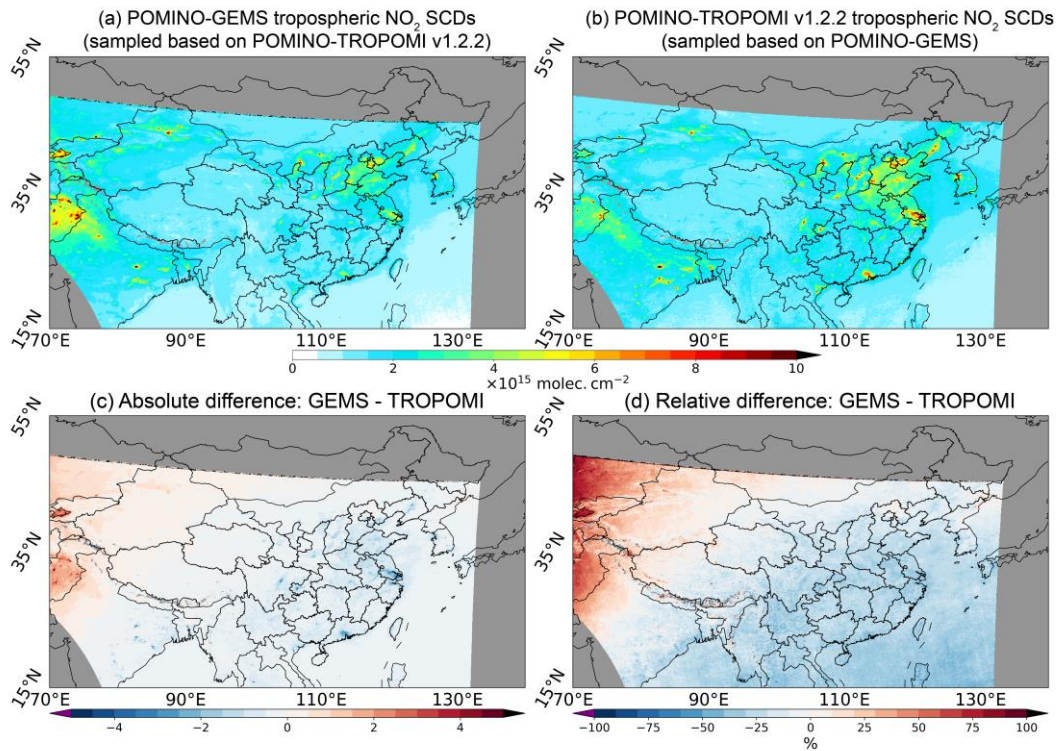
156



157

158 **Figure S12. Spatial distribution of (a) POMINO-GEMS and (b) POMINO-TROPOMI v1.2.2 tropospheric**
 159 **NO₂ scattering correction factors on a 0.05° × 0.05° grid in JJA 2021. (c) and (d) are absolute and relative**
 160 **differences of POMINO-GEMS tropospheric NO₂ scattering correction factors from those of POMINO-**
 161 **TROPOMI v1.2.2, respectively. Data are sampled from locations and times with valid NO₂ VCD data in**
 162 **both POMINO-GEMS and POMINO-TROPOMI v1.2.2. The regions in grey mean there are no valid NO₂**
 163 **observations.**

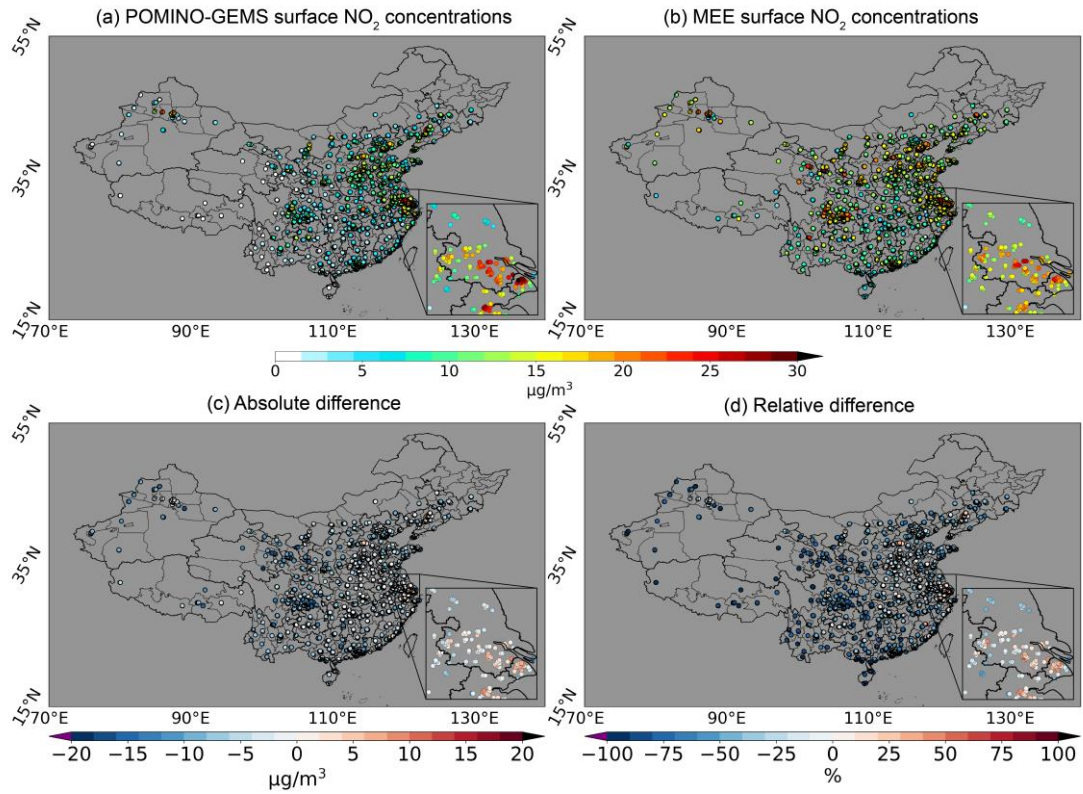
164



165

166 **Figure S13. Spatial distribution of (a) POMINO-GEMS and (b) POMINO-TROPOMI v1.2.2 tropospheric**
 167 **NO₂ SCDs on a 0.05° × 0.05° grid in JJA 2021. (c) and (d) are absolute and relative differences of POMINO-**
 168 **GEMS tropospheric NO₂ SCDs from those of POMINO-TROPOMI v1.2.2, respectively. Data are sampled**
 169 **from locations and times with valid NO₂ VCD data in both POMINO-GEMS and POMINO-TROPOMI**
 170 **v1.2.2. The regions in grey mean there are no valid NO₂ observations.**

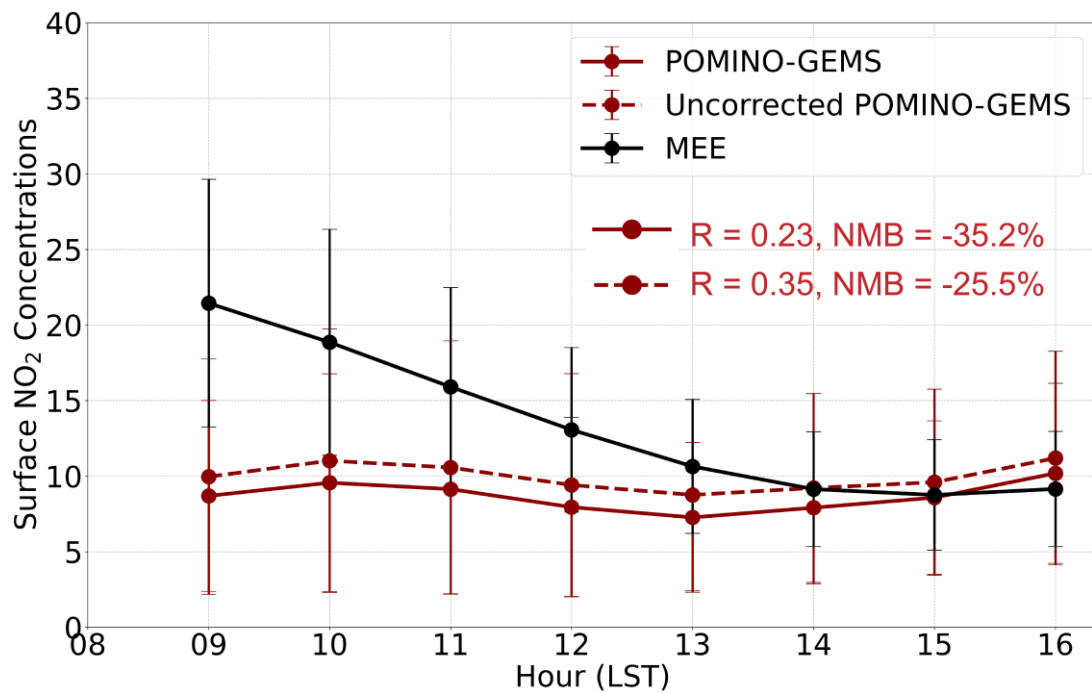
171



172

173 **Figure S14. Evaluation of POMINO-GEMS derived surface NO₂ concentrations. Mean surface NO₂**
 174 **concentrations (a) derived from POMINO-GEMS VCDs and (b) taken from MEE measurements in JJA**
 175 **2021. Panels (c) and (d) are the absolute and relative differences of POMINO-GEMS relative to MEE. The**
 176 **sub-figures show a zoomed-in map around the Yangtze River Delta (YRD) region (118-122°E, 30-34°N).**

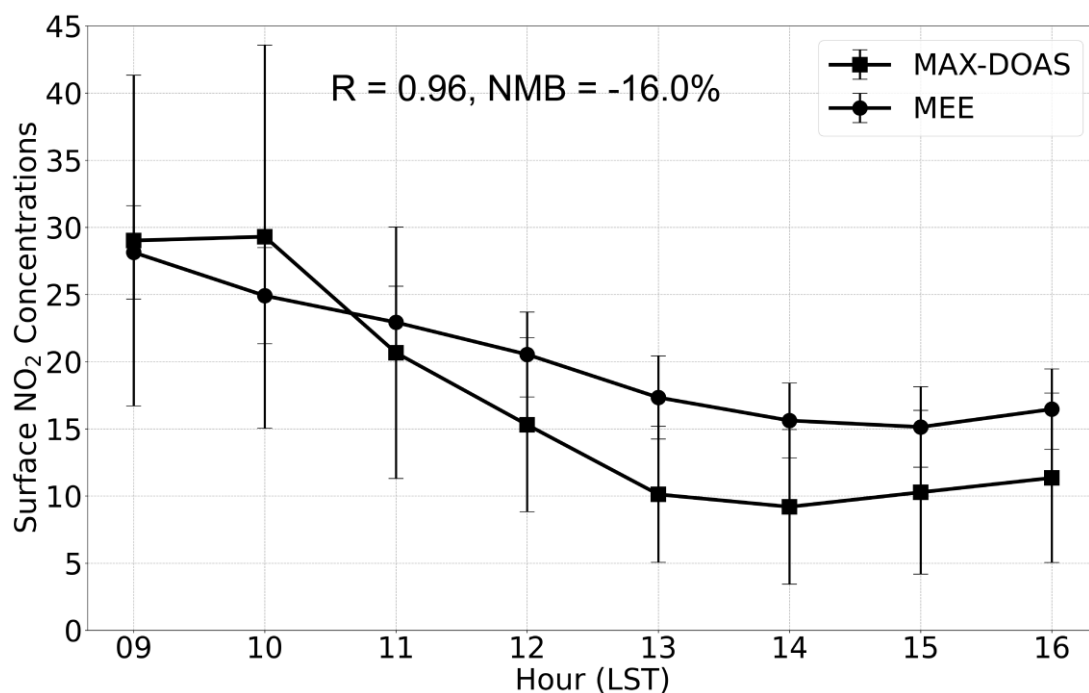
177



178

179 Figure S15. Diurnal variation of hourly surface NO₂ concentrations (µg m⁻³) of MEE (back line), POMINO-
 180 GEMS with TROPOMI correction (red solid line) and without TROPOMI correction (red dashed line)
 181 using daily GEOS-Chem column-to-surface ratios in JJA 2021. The error bars denote the standard
 182 deviation of MEE and POMINO-GEMS derived surface NO₂ concentrations at each hour in JJA 2021,
 183 respectively. Values for diurnal correlation and mean NMB of POMINO-GEMS relative to MEE data are
 184 shown.

185



186

187 Figure S16. Diurnal variation of hourly surface NO₂ concentrations (µg m⁻³) for MEE (circle marks) and
 188 MAX-DOAS (square marks) in JJA 2021. The error bars denote the standard deviation of MEE and MAX-
 189 DOAS derived surface NO₂ concentrations at each hour in JJA 2021, respectively. Values for diurnal
 190 correlation and mean NMB of MAX-DOAS derived surface NO₂ concentrations relative to MEE data are
 191 shown.

192 **References**

- 193 Bogumil, K., Orphal, J., Homann, T., Voigt, S., Spietz, P., Fleischmann, O. C., Vogel, A., Hartmann, M.,
194 Kromminga, H., Bovensmann, H., Frerick, J., and Burrows, J. P.: Measurements of molecular absorption
195 spectra with the SCIAMACHY pre-flight model: instrument characterization and reference data for
196 atmospheric remote-sensing in the 230–2380 nm region, *Journal of Photochemistry and Photobiology A:
197 Chemistry*, 157, 167-184, [https://doi.org/10.1016/S1010-6030\(03\)00062-5](https://doi.org/10.1016/S1010-6030(03)00062-5), 2003.
- 198 Chance, K. and Kurucz, R. L.: An improved high-resolution solar reference spectrum for earth's
199 atmosphere measurements in the ultraviolet, visible, and near infrared, *Journal of Quantitative
200 Spectroscopy and Radiative Transfer*, 111, 1289-1295, <https://doi.org/10.1016/j.jqsrt.2010.01.036>, 2010.
- 201 Chance, K. V. and Spurr, R. J. D.: Ring effect studies: Rayleigh scattering, including molecular
202 parameters for rotational Raman scattering, and the Fraunhofer spectrum, *Appl. Opt.*, 36, 5224-5230,
203 10.1364/AO.36.005224, 1997.
- 204 Choi, Y., Kanaya, Y., Takashima, H., Irie, H., Park, K., and Chong, J.: Long-Term Variation in the
205 Tropospheric Nitrogen Dioxide Vertical Column Density over Korea and Japan from the MAX-DOAS
206 Network, 2007–2017, *Remote Sensing*, 13, 1937, 10.3390/rs13101937, 2021.
- 207 Clémer, K., Van Roozendael, M., Fayt, C., Hendrick, F., Hermans, C., Pinardi, G., Spurr, R., Wang, P.,
208 and De Mazière, M.: Multiple wavelength retrieval of tropospheric aerosol optical properties from
209 MAXDOAS measurements in Beijing, *Atmospheric Measurement Techniques*, 3, 863-878, 10.5194/amt-
210 3-863-2010, 2010.
- 211 Hendrick, F., Müller, J.-F., Clémer, K., Wang, P., De Mazière, M., Fayt, C., Gielen, C., Hermans, C., Ma,
212 J. Z., Pinardi, G., Stavrakou, T., Vlemmix, T., and Van Roozendael, M.: Four years of ground-based
213 MAX-DOAS observations of HONO and NO₂ in the Beijing area, *Atmospheric Chemistry
214 and Physics*, 14, 765-781, 10.5194/acp-14-765-2014, 2014.
- 215 Kanaya, Y., Irie, H., Takashima, H., Iwabuchi, H., Akimoto, H., Sudo, K., Gu, M., Chong, J., Kim, Y. J.,
216 Lee, H., Li, A., Si, F., Xu, J., Xie, P.-H., Liu, W.-Q., Dzhola, A., Postlyakov, O., Ivanov, V., Grechko,
217 E., Terpugova, S., and Panchenko, M.: Long-term MAX-DOAS network observations of
218 NO₂ in Russia and Asia (MADRAS) during the period 2007–2012: instrumentation,
219 elucidation of climatology, and comparisons with OMI satellite observations and global model si,
220 *Atmospheric Chemistry and Physics*, 14, 7909-7927, 10.5194/acp-14-7909-2014, 2014.

221 Liu, M., Lin, J., Kong, H., Boersma, K. F., Eskes, H., Kanaya, Y., He, Q., Tian, X., Qin, K., Xie, P., Spurr,
222 R., Ni, R., Yan, Y., Weng, H., and Wang, J.: A new TROPOMI product for tropospheric NO₂ columns
223 over East Asia with explicit aerosol corrections, *Atmos. Meas. Tech.*, 13, 4247-4259, 10.5194/amt-13-
224 4247-2020, 2020.

225 Liu, M., Lin, J., Boersma, K. F., Pinardi, G., Wang, Y., Chimot, J., Wagner, T., Xie, P., Eskes, H., Van
226 Roozendaal, M., Hendrick, F., Wang, P., Wang, T., Yan, Y., Chen, L., and Ni, R.: Improved aerosol
227 correction for OMI tropospheric NO₂ retrieval over East Asia: constraint from CALIOP aerosol vertical
228 profile, *Atmospheric Measurement Techniques*, 12, 1-21, 10.5194/amt-12-1-2019, 2019.

229 Pope, R. M. and Fry, E. S.: Absorption spectrum (380–700 nm) of pure water. II. Integrating cavity
230 measurements, *Appl. Opt.*, 36, 8710-8723, 10.1364/AO.36.008710, 1997.

231 Serdyuchenko, A., Gorshchev, V., Weber, M., Chehade, W., and Burrows, J. P.: High spectral resolution
232 ozone absorption cross-sections – Part 2: Temperature dependence, *Atmos. Meas. Tech.*, 7, 625-
233 636, 10.5194/amt-7-625-2014, 2014.

234 Thalman, R. and Volkamer, R.: Temperature dependent absorption cross-sections of O₂–O₂ collision
235 pairs between 340 and 630 nm and at atmospherically relevant pressure, *Physical Chemistry Chemical
236 Physics*, 15, 15371-15381, 10.1039/C3CP50968K, 2013.

237 Vandaele, A. C., Hermans, C., Simon, P. C., Carleer, M., Colin, R., Fally, S., Mérienne, M. F., Jenouvrier,
238 A., and Coquart, B.: Measurements of the NO₂ absorption cross-section from 42 000 cm⁻¹ to 10 000
239 cm⁻¹ (238–1000 nm) at 220 K and 294 K, *Journal of Quantitative Spectroscopy and Radiative Transfer*,
240 59, 171-184, [https://doi.org/10.1016/S0022-4073\(97\)00168-4](https://doi.org/10.1016/S0022-4073(97)00168-4), 1998.

241 Zhang, R., Wang, S., Zhang, S., Xue, R., Zhu, J., and Zhou, B.: MAX-DOAS observation in the
242 midlatitude marine boundary layer: Influences of typhoon forced air mass, *Journal of Environmental
243 Sciences*, 120, 63-73, <https://doi.org/10.1016/j.jes.2021.12.010>, 2022a.

244 Zhang, S., Wang, S., Xue, R., Zhu, J., Tanvir, A., Li, D., and Zhou, B.: Impact Assessment of COVID-19
245 Lockdown on Vertical Distributions of NO₂ and HCHO From MAX-DOAS Observations and Machine
246 Learning Models, *Journal of Geophysical Research: Atmospheres*, 127, e2021JD036377,
247 <https://doi.org/10.1029/2021JD036377>, 2022b.

248 Zhang, S., Wang, S., Zhang, R., Guo, Y., Yan, Y., Ding, Z., and Zhou, B.: Investigating the Sources of
249 Formaldehyde and Corresponding Photochemical Indications at a Suburb Site in Shanghai From MAX-

250 DOAS Measurements, *Journal of Geophysical Research: Atmospheres*, 126, e2020JD033351,
251 <https://doi.org/10.1029/2020JD033351>, 2021.

252 Zhu, J., Wang, S., Dao, X., Liu, D., Wang, J., Zhang, S., Xue, R., Tang, G., and Zhou, B.: Comparative
253 observation of aerosol vertical profiles in urban and suburban areas: Impacts of local and regional
254 transport, *Science of The Total Environment*, 805, 150363,
255 <https://doi.org/10.1016/j.scitotenv.2021.150363>, 2022.

256